

Enhancement of Signal Intensity for Inverse Photoelectron Spectroscopy by Surface Plasmon Resonance of Ag nanoparticles

Ryota Usui¹, Hiroyuki Yoshida^{1,2,}*

¹ Graduate School of Engineering, Chiba University, 1-33 Yayoi-cho, Inage-ku, Chiba 263-8522, Japan

² Molecular Chirality Research Center, Chiba University, 1-33 Yayoi-cho, Inage-ku, Chiba 263-8522, Japan

*Corresponding Author E-mail: hyoshida@chiba-u.jp

ORCID Hiroyuki Yoshida: 0000-0002-8889-324

ABSTRACT

Information concerning the unoccupied states of condensed matter is of great relevance to their electronic, optical and chemical properties. These unoccupied states can be directly examined by inverse photoelectron spectroscopy (IPES), which is often regarded as the time-inversion process of photoelectron spectroscopy (PES). The fundamental drawback of IPES is its low signal intensity. Other spectroscopic intensities are enhanced by surface plasmon resonance (SPR), so the intensity of the IPES signal may also be enhanced by SPR. This was, however, impossible because the photon energy involved in conventional IPES exceeds 9 eV and is much higher than the SPR energy of existing materials. In 2012, we developed low-energy IPES (LEIPS), in which the photon energy is less than 5 eV, which can then be matched with the SPR energy. We demonstrate a 5-fold enhancement of the LEIPS signal from a prototypical organic semiconductor, copper phthalocyanine (CuPc), by SPR of Ag nanoparticles.

KEYWORDS

surface plasmon resonance, inverse photoelectron spectroscopy, unoccupied states, electron affinity, organic semiconductor, silver nanoparticle

Electronic, optical and chemical properties of solids are governed by the electronic structure of both occupied and unoccupied states. The occupied states (or the valence bands) are usually examined by photoelectron spectroscopy (PES). The unoccupied states (or the conduction bands) are best examined by inverse photoelectron spectroscopy (IPES)¹. In IPES, an electron is introduced to the sample surface and a photon is emitted, owing to the radiative transition from the free electron state to the unoccupied states. By measuring the photons, the energy of the unoccupied states can be obtained from the kinetic energy of the introduced electron and the energy of the emitted photon. IPES is complimentary to and often regarded as the time inversion process of PES.

In contrast to PES being routinely used to examine the occupied states, IPES is far less common. The fundamental drawback is the low signal intensity (cross-section). According to the theoretical consideration, the cross section of IPES is 3 and 5 orders of magnitude smaller than that of PES²⁻³. To obtain a reasonable signal-to-noise ratio, the weak photon signal is detected by a high sensitivity bandpass photon detector⁴. The photon detector specially-designed for IPES limits the energy of the photon in the range between 9 and 10 eV (around 130 nm in wavelength) and the energy resolution as high as 0.5 eV when reasonable signal intensity is acquired. The sufficient signal intensity is also gained by introducing an intense electron beam to the sample. The bombardment by the intense electron beam can cause serious damage to soft-materials such as organic semiconductors and bio-related molecules. If the IPES signal can be intensified, the application of this experimental technique should be greatly extended.

To enhance the signal intensity, surface plasmon resonance (SPR) is a promising candidate. Surface plasmon is a collective oscillation of the free electrons supported at the interface between a metal surface and a dielectric. When a photon is coupled with the surface plasmon, electromagnetic field is strongly enhanced. This effect is called SPR⁵. SPR enhances the signal intensity of the spectroscopic techniques involving photons. For example, the signal intensity is intensified by orders of magnitudes in Raman spectroscopy⁶⁻⁸ and fluorescence spectroscopy⁹. The enhancement has also been reported in infrared spectroscopy¹⁰, sum frequency generation (SHG)¹¹, and PES¹². SPR is routinely used in biosensors¹³⁻¹⁴ or other practical applications.

To combine IPES and SPR, the SPR frequency must be matched with the IPES photon frequency ω . SPR has the propagation and the localized modes, and its frequency ω_{sp} is variable of the size and shape of the metal structures and dielectric. In any case, ω_{sp} is always smaller than $\omega_p/\sqrt{2}$ where ω_p is the bulk plasmon frequency¹⁵. To date, SPR energy $\hbar\omega$ above 6 eV (below 200 nm in wavelength) have been difficult to obtain¹⁶. In conventional IPES, the photon energy between 9 and 10 eV is detected (around 130 nm). Unfortunately, therefore, the IPES signal is not able to be enhanced by SPR.

In 2012, we developed an advanced IPES called low-energy inverse photoelectron spectroscopy (LEIPS, Figure 1a)¹⁷⁻¹⁹. The initial aim of LEIPS was to prevent damage to the organic semiconductor molecules arising from the electron bombardment. For this purpose, the kinetic energy of the incident electron is kept less than 5 eV, which is the typical damage threshold of molecules. As a result, the energy of the emitted photons becomes less than 5 eV (more than 250 nm in wavelength) for most materials. The detection wavelength in the range between 250 nm and 500 nm can be matched with the SPR wavelength of Ag. Furthermore, in the standard LEIPS setup, optical bandpass filters are used for photon detection¹⁷. The photon energy can be tuned by changing the bandpass filters so that the LEIPS wavelength can be easily matched with the SPR wavelength. Note that the spectral scan of IPES can be made with two modes, namely the tunable photon energy (TPE) and isochromat modes¹⁹. In TPE mode, the kinetic energy of incident electron is fixed and the photon energy is scanned. Since the SPR enhancement sensitively depends on the wavelength, the LEIPS spectrum will be distorted in the TPE mode. The isochromat mode, on the other hand, scans the electron energy with detecting photons at a fixed energy using the bandpass photon detector. If the detection wavelength is matched with the SPR wavelength, the entire spectral energy region is evenly enhanced.

The concept of this study is shown in Figure 1. We adopted Ag nanoparticles for the SPR media. First, we prepared silver (Ag) nanoparticles using vacuum deposition and characterized such basic properties as particle shape and SPR wavelength using atomic force microscopy (AFM) and extinction spectroscopy, respectively. Second, we observed the enhancement of the LEIPS signal intensity of the Ag nanoparticles. Third, we enhanced the LEIPS signal of a prototypical organic semiconductor, copper phthalocyanine (CuPc, Figure 1d). Throughout the work, the enhancements by SPR were confirmed by (1) comparing the intensities with and without the Ag nanoparticle, and (2) measuring LEIPS spectra as a function of photon energy for comparison with the extinction spectra.

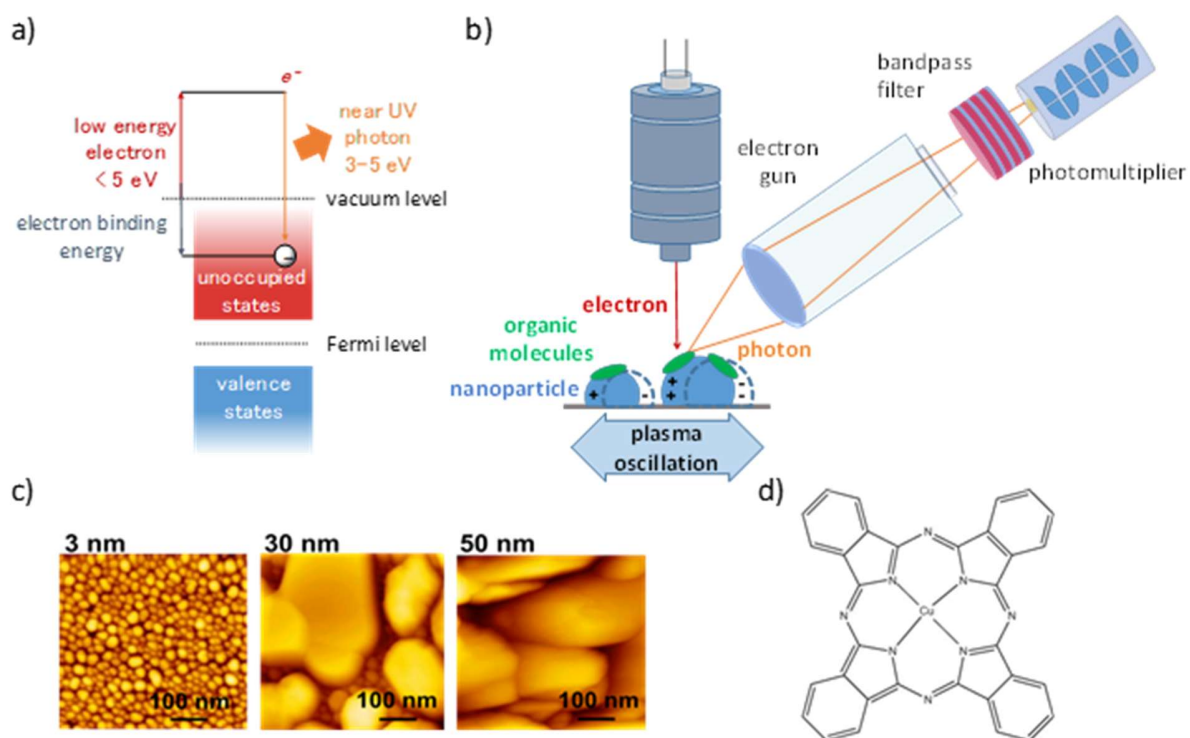


Figure 1. Concept of the present work. The signal of low energy inverse photoelectron spectroscopy (LEIPS) is enhanced by the surface plasmon resonance (SPR) of metal nanoparticles. (a) Energy level diagram of LEIPS. (b) Experimental setup. The LEIPS signal of the metal nanoparticle as well as the organic molecules will be enhanced by the SPR of the metal nanoparticles. (c) AFM images of Ag deposited on the ITO substrates with average thicknesses of 3, 30 and 50 nm. (d) Molecular structure of Cu-phthalocyanine.

Figure 1c shows the AFM images of Ag nano-particles with average Ag-thicknesses of 3 nm, 30 nm and 50 nm (denoted as Ag3, Ag30 and Ag50, respectively, hereafter). The average particle size and the average height were 25 nm and 10 nm for Ag3, 160 nm and 75 nm for Ag30, and 200 nm and 80 nm for Ag50. Figure 2c shows the extinction spectra of the Ag nanoparticles (see Figure S1 in the Supporting Information). Since the ITO/glass substrate does not transmit ultraviolet light, we show only the extinction spectra at wavelengths longer than 320 nm. The broad peaks attributable to SPR were observed at 567 nm for Ag3, 383 nm for Ag30, and 454 nm for Ag50.

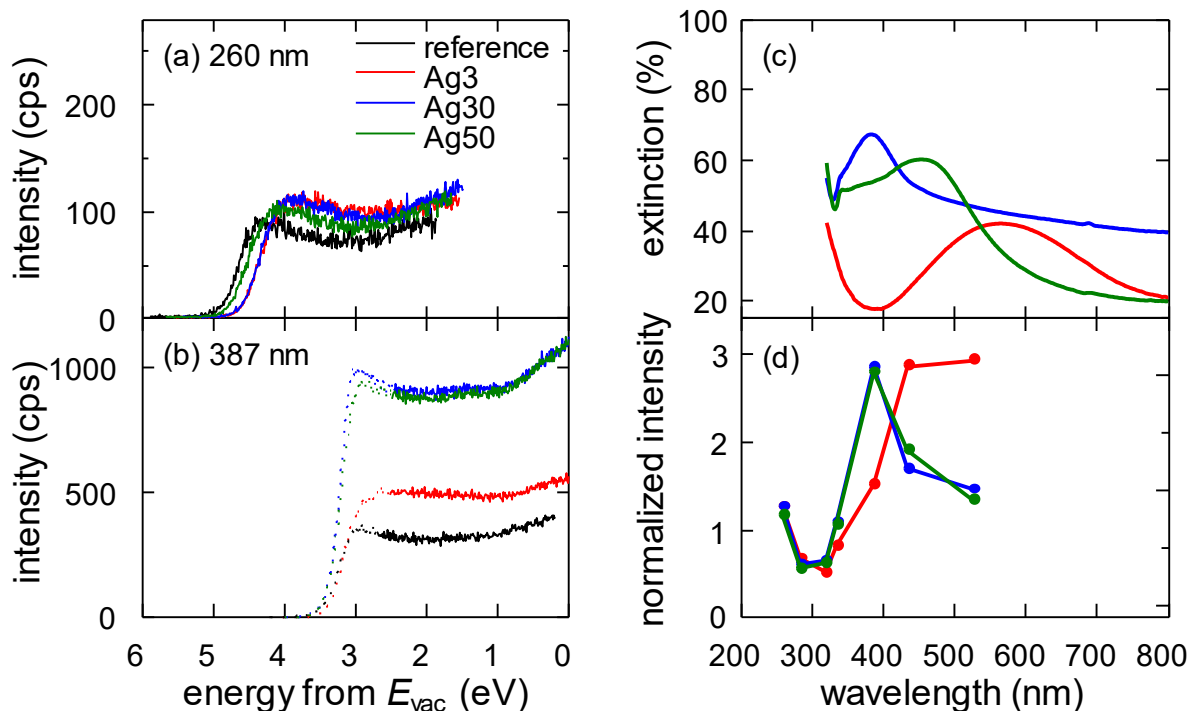


Figure 2. LEIPS and SPR data of Ag nanoparticles on the ITO. LEIPS spectra taken at the detection wavelength of (a) 260 nm and (b) 387 nm. A silver plate was measured as a reference. The onset regions inaccessible by the 387-nm photons are indicated by dotted lines (see text). Comparison of (c) extinction spectra and (d) wavelength-dependence of LEIPS intensity.

Figure 2a and 2b show the LEIPS spectra of Ag nanoparticles measured at the detection wavelengths of 260 nm and 387 nm. The onset energy corresponds to the workfunction of each sample at 260 nm. The subtle differences in the onset energy is owing to the sample-to-sample variation of the workfunctions. On the other hand, the Fermi edge cannot be accessed by LEIPS at 387 nm because the photon energy (3.2 eV) is smaller than the workfunction of the samples (typically 4.5 eV). The onset observed at 387 nm arises from the sudden increase of the electron beam current when the electron energy exceeds the vacuum.

At 260 nm, the LEIPS intensities were almost the same as each other. However, at 387 nm, the LEIPS intensity of Ag3 was approximately 1.2 times, whereas those of Ag30 and Ag50 were approximately 3 times more intense than that of the reference. Since the LEIPS intensity varies depending on the detection wavelength, we investigated the wavelength dependence of the LEIPS intensity, as shown in Figure 2d. The intensity was determined as the area of the LEIPS spectrum with an energy between 1 and 2 eV above the onset. The peak of the LEIPS intensity was observed at the detection wavelength of 525 nm for Ag3, while the peak of the LEIPS signal peaked around 387 nm for Ag30 and Ag50. Since the extinction spectra in Figure 2c and the wavelength

dependence of the LEIPS intensity in Figure 2d were similar to each other, we concluded that the enhancement of LEIPS intensity was caused by SPR.

Now that we observed the enhancement of the Ag signal arising from SPR, we attempted to enhance the LEIPS signal from an organic semiconductor, CuPc, as the next step. The LEIPS spectrum of CuPc/Ag can be regarded as the superposition of the Ag nanoparticle and CuPc ¹⁷ spectra, as shown in Figure S3 in the Supporting Information. The spectrum of the Ag nanoparticle was subtracted from the observed spectrum (Figure S4) and the spectral component of CuPc was obtained, as shown in Figure 3. The LEIPS intensities of CuPc on the Ag nanoparticles were the same as that of the reference within the uncertainties at the detection wavelength of 260 nm (Figure 3a). At the detection wavelength of 434 nm (Figure 3b), however, the LEIPS intensities of CuPc on Ag30 and Ag50 were 3 and 5 times larger than that of the reference, respectively, while no enhancement was observed for CuPc/Ag3. Note that slight differences in the energy were observed. For example, the onsets of the spectra corresponding to the electron affinities (EAs), were 3.10 eV (CuPc/ITO, reference), 3.35 eV (CuPc/Ag3), 3.18 eV (CuPc/Ag30), and 3.39 eV (CuPc/Ag50). It has been reported that the energy levels of CuPc depend on the molecular orientation; the ionization energy for the stand-up and lying-down orientations differ by 0.4 eV ²⁰. In general, CuPc molecules tend to adopt the stand-up orientation on the ITO and the lying-down orientation on the metal surfaces ²¹. The variations in energy were therefore attributed to the differences in the molecular orientations of CuPc on ITO and Ag nanoparticles. To determine the electron affinities precisely, such energy shift induced by nanoparticles are undesirable. The molecular orientation of molecules on the nanoparticle could be controlled by covering the metal nanoparticles by a thin layer of another material e.g. SiO₂ ²².

If the enhancement occurs as a result of SPR, we would expect a good correlation between the wavelength-dependence of the LEIPS signal and the SPR wavelength (extinction spectra), similar to the case of the pristine Ag nanoparticles. Figure 3c shows the extinction spectra of CuPc / Ag nanoparticles. Since each extinction spectrum contains contributions from both the SPR of Ag nanoparticles and the CuPc molecular absorption, we subtracted the separately-measured CuPc spectrum from the observed extinction spectrum (Figure S2 in Supporting Information). The extinction spectra showed broad features owing to the SPR peak at around 497 nm for CuPc/Ag3, 477 nm for CuPc/Ag30, and 522 nm for CuPc/Ag50. The differences in the spectra with and without the CuPc layer could be attributed to the higher permittivity (approximately 3 ²³) than the vacuum. Additionally, an energy shift might have been imposed by further oxidation of the surface of Ag nanoparticles in the latter samples as we used the same Ag nanoparticles stored in air for the pristine Ag and CuPc-deposited experiments.

Figure 3d shows the LEIPS intensity as a function of the detection wavelength. We assumed the area of the 1st peak as the spectral intensity. While no wavelength dependence was observed in CuPc/Ag3, the signal intensities increased at longer wavelength until the longest wavelength we measured in the present work; at 434 nm, the signal intensities were 3.4 and 5.8 times more intense than the reference for CuPc/Ag30 and CuPc/Ag50, respectively. Comparing the wavelength

dependence of the LEIPS intensity with the extinction spectra in panels c and d in Figure 3, we concluded that the enhancement of the LEIPS signal was caused by SPR.

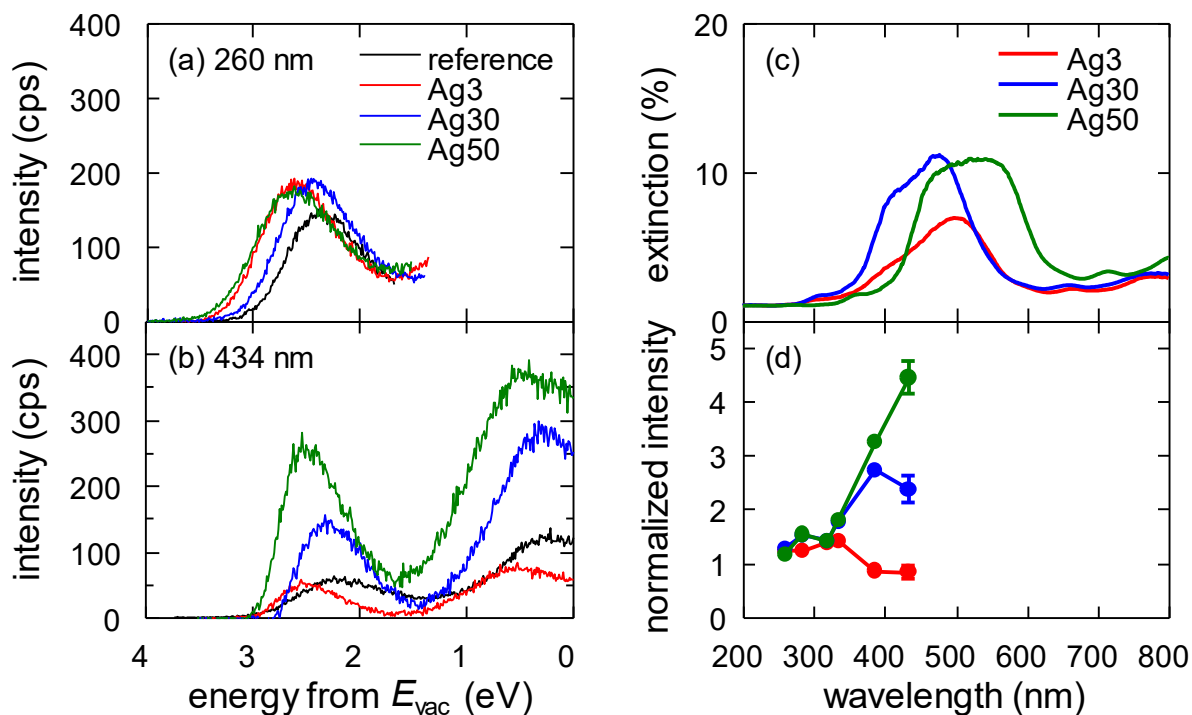


Figure 3. LEIPS spectra of 20-nm-thick CuPc on Ag nanoparticles measured at the detection wavelengths of (a) 260 nm and (b) 434 nm. The spectral component from the Ag nanoparticles are subtracted. Comparison of (c) extinction spectra of 40-nm-thick CuPc fabricated on Ag nanoparticles and (d) wavelength-dependence of LEIPS intensity of 20-nm-thick CuPc fabricated on Ag nanoparticles.

To evaluate the penetration depth of SPR into the organic layer from the surface of the Ag nanoparticles, we performed the CuPc-thickness dependent experiment. Figure 4 shows the CuPc-thickness dependence of the CuPc spectral components from which the penetration depth of the SPR could be evaluated. No thickness-dependence was observed for CuPc/Ag3, which could be explained by the absence of an SPR effect in CuPc/Ag3. However, the intensities of CuPc/Ag30 and CuPc/Ag50 decreased as the CuPc film thickness increased. By fitting exponential decay functions²⁴ to the experimental data, as shown in Figure 4, the penetration depths of SPR (the value at which the signal strength becomes the reciprocal of Euler's number, $1/e$) were 8.4 nm for Ag30 and 10 nm for Ag50. In this argument, we assumed that the probing depth of LEIPS is sufficiently smaller than the penetration depth of SPR. The probing depth of LEIPS is governed by the inelastic mean free path of electrons. In the energy of electrons below 10 eV, there are only few reports about the mean free path of electrons in organic materials and are estimated to be a few nm²⁵⁻²⁷.

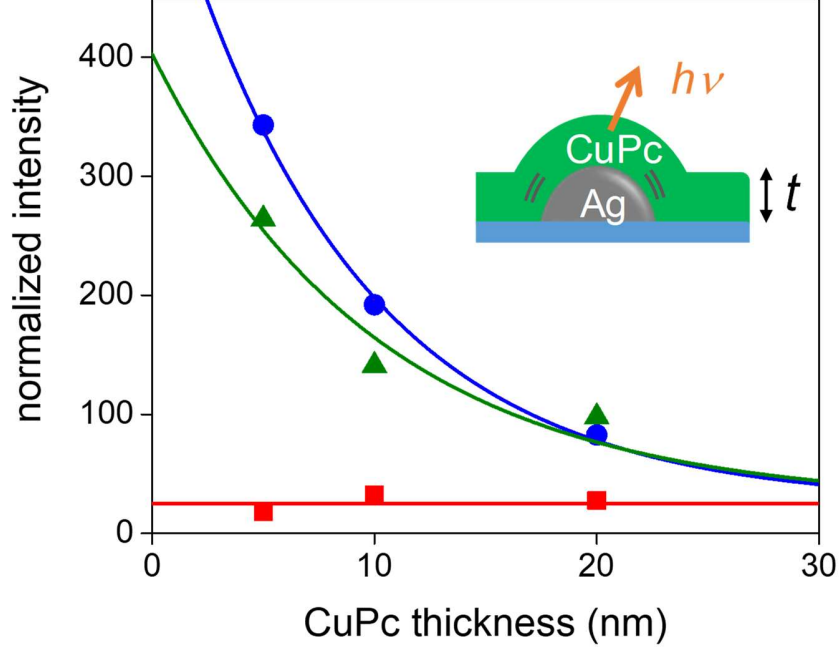


Figure 4. Thickness dependence of LEIPS intensities from the CuPc layers of CuPc/Ag. Experimental data are shown by dots and the best-fit results by exponential functions are shown by solid lines (Ag3 in red, Ag30 in blue, and Ag50 in green).

Finally, we considered the origin of the enhancement of the LEIPS intensity arising from SPR. The signal enhancement by SPR involves the system absorbing a photon and emitting a photon (photon-in/photon-out); for examples, Raman spectroscopy, fluorescence spectroscopy, and SHG; or absorbing a photon and emitting an electron (photon-in/electron out); for examples, photoelectron spectroscopy, and two-photon photoelectron spectroscopy (2PPE). The effect of the photon can be treated by the classical time-dependent perturbation theory. Based on this classical picture, the enhancement of the spectroscopic signal intensity can be intuitively understood as the coupling between the electric fields of photon and SPR. In contrast, an electron is introduced to a system and a photon is created (electron-in/photon-out) in IPES in which the electromagnetic field should be quantized²⁻³. This process is similar to the photon emission from the scanning tunneling microscope (STM)²⁸⁻²⁹ and light-emitting diodes³⁰.

The total decay rate of PES process with the transition matrix element $\langle b | \vec{\epsilon} \cdot \mathbf{p} | k \rangle$ from a free electron state $|k\rangle$ to a bound state $|b\rangle$ can be represented by Fermi's golden rule as^{2-3, 31},

$$\Gamma = \frac{\pi\omega}{3\hbar\epsilon_0} |\langle b | \vec{\epsilon} \cdot \mathbf{p} | k \rangle|^2 \rho_p \quad (1)$$

where ρ_p is the density of states (DOS) of the photon, while \hbar refers to the reduced Planck constant. The DOS of the photon ρ_p is increased by SPR owing to the deviation of the dispersion relation from the light-line in the propagation mode⁵ or increase of the local density of electromagnetic states (LDOS) in the localized mode³¹. The increase of the DOS of the photon causes an increase of the IPES signal intensity.

In summary, we have observed the enhancement of the low-energy IPES (LEIPS) signal by the SPR of Ag nanoparticles. First, we examined the LEIPS intensity of the Ag nanoparticles and successfully observed an enhancement by a factor of 3. Then, by using the Ag nanoparticles, we achieved between a 3- to 5-fold enhancement of the LEIPS signal of a prototypical organic semiconductor, copper phthalocyanine (CuPc). Since the wavelength dependence of the enhancement of the LEIPS intensities and the extinction spectra coincided with each other, the enhancement of the LEIPS intensity was confirmed to arise from the SPR of Ag nanoparticles. The enhancement of the LEIPS signal intensity was caused by the increase of the density of states of the photon arising from SPR, which indicates that a further enhancement is feasible by increasing the DOS of photons.

EXPERIMENTAL METHODS

We used indium-tin-oxide (ITO) coated glass (Geomatic, Flat ITO) as a substrate because it has electrical conduction and is transparent to visible light, which were necessary to prevent sample charging in the LEIPS measurement and to investigate the SPR wavelength, respectively. Ag was vacuum deposited onto the substrate at room temperature under a pressure of 6.0×10^{-5} Pa to produce Ag nanoparticles. The average film thickness was monitored by a quartz crystal microbalance. The deposition rate was kept at 0.30 nm min^{-1} and the average film thicknesses were 3, 30, and 50 nm. For the organic material, copper (II) phthalocyanine (Sigma-Aldrich) was purified by vacuum sublimation and deposited at a rate of 0.15 nm min^{-1} to obtain films with an average film thickness ranging between 0 and 40 nm. For the reference of the signal intensities of Ag nanoparticles and CuPc on Ag nanoparticles, a flat Ag plate and CuPc deposited on a bare ITO/glass were employed, respectively.

The shapes of Ag nanoparticles were observed by an atomic force microscope (AFM; SEIKO Instruments, SPA-400) in atmosphere. The SPR properties of the Ag nanoparticles were examined from their extinction spectra. We measured the transmittance and reflectance spectra with a UV-vis spectrophotometer (JASCO V-650) equipped with an integrating sphere (JASCO ISV-722). The extinction ratio was calculated by the procedure described in the Supporting Information.

The prepared sample was exposed to air and introduced to a LEIPS apparatus. The LEIPS setup for the isochromat mode has been described elsewhere³². An electron beam with a current of $0.3 \mu\text{A}$ was incident to the sample surface and the emitted photons were analyzed using a bandpass

filter and a photomultiplier. The pressure during the LEIPS measurement was 3.0×10^{-8} Pa. We used the bandpass filters with center wavelengths of transmittance at 260, 285, 300, 320, 335, 387, 434, and 525 nm. The throughput of the bandpass filters, the sensitivity of the photomultiplier and the collection efficiency of the focusing lens depended on the wavelength. The LEIPS intensities were calibrated with that of a CuPc film of 20 nm thickness deposited on ITO taken with each bandpass filter.

SUPPORTING INFORMATION

The Supporting Information is available free of charge on the ACS Publications website at XXXXX. Evaluation method of extinction spectra, extinction spectra of CuPc/Ag nanoparticles, LEIPS spectra of CuPc/Ag and derivation of CuPc contributions.

NOTES

The authors declare no competing financial interest.

ACKNOWLEDGEMENTS

We would like to thank Dr. K. Tajima of RIKEN and Prof. H. Ishii of Chiba University for allowing us to use the UV-vis spectrophotometer and AFM, respectively. This work was supported by JSPS KAKENHI Grant-in-Aid for Challenging Exploratory Research (Grant Number 16K13924).

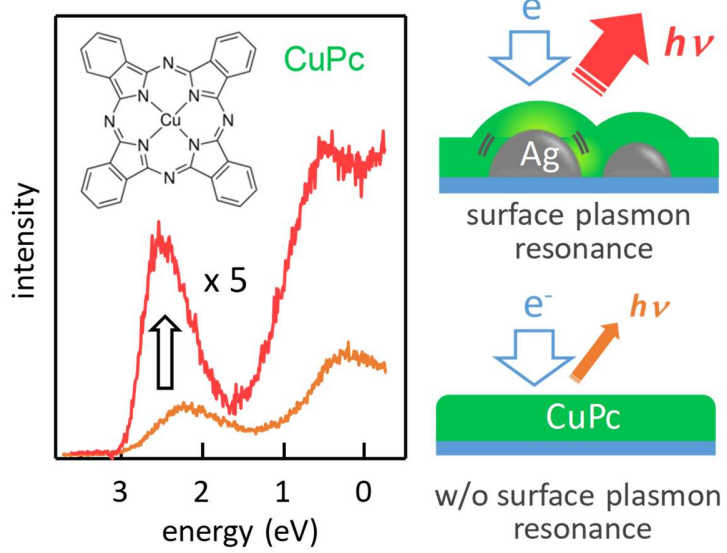
REFERENCES

1. Hüfner, S., Photoelectron Spectroscopy: Principles and Applications. Springer: 2003.
2. Pendry, J., New Probe for Unoccupied Bands at Surfaces. *Phys. Rev. Lett.* **1980**, *45*, 1356.
3. Johnson, P.; Davenport, J., Calculated Inverse Photoemission Cross Sections from Adsorbed Molecules. *Phys. Rev. B* **1985**, *31*, 7521.
4. Denninger, G.; Dose, V.; Scheidt, H., Vuv Isochromat Spectrometer for Surface-Analysis. *Applied Physics* **1979**, *18*, 375-380.
5. Raether, H., Surface Plasmons on Smooth Surfaces. In *Surface Plasmons on Smooth and Rough Surfaces and on Gratings*, Springer: 1988.
6. Fleischmann, M.; Hendra, P. J.; McQuillan, A. J., Raman Spectra of Pyridine Adsorbed at a Silver Electrode. *Chemical Physics Letters* **1974**, *26*, 163-166.
7. McQuillan, A.; Hendra, P.; Fleischmann, M., Raman Spectroscopic Investigation of Silver Electrodes. *J. Electroanal. Chem. Interfacial Electrochem.* **1975**, *65*, 933-944.
8. Paul, R.; McQuillan, A.; Hendra, P.; Fleischmann, M., Laser Raman Spectroscopy at the Surface of a Copper Electrode. *J. Electroanal. Chem. Interfacial Electrochem.* **1975**, *66*, 248-249.
9. Liebermann, T.; Knoll, W., Surface-Plasmon Field-Enhanced Fluorescence Spectroscopy. *Colloids Surf. A* **2000**, *171*, 115-130.
10. Osawa, M., Dynamic Processes in Electrochemical Reactions Studied by Surface-Enhanced Infrared Absorption Spectroscopy (Seiras). *Bull. Chem. Soc. Japan* **1997**, *70*, 2861-2880.
11. Baldelli, S.; Eppler, A. S.; Anderson, E.; Shen, Y.-R.; Somorjai, G. A., Surface Enhanced Sum Frequency Generation of Carbon Monoxide Adsorbed on Platinum Nanoparticle Arrays. *J. chem. phys.* **2000**, *113*, 5432-5438.
12. Ono, A.; Shiroshita, N.; Kikawada, M.; Inami, W.; Kawata, Y., Enhanced Photoelectron Emission from Aluminum Thin Film by Surface Plasmon Resonance under Deep-Ultraviolet Excitation. *J. Phys. D : Appl. Phys.* **2014**, *48*, 184005.
13. Homola, J.; Yee, S. S.; Gauglitz, G., Surface Plasmon Resonance Sensors. *Sens. Actuators B Chem.* **1999**, *54*, 3-15.
14. Cartier, E.; Pfluger, P., Transport and Relaxation of Hot Conduction Electrons in an Organic Dielectric. *Phys. Rev. B* **1986**, *34*, 8822-8827.
15. Kreibig, U.; Zacharias, P., Surface Plasma Resonances in Small Spherical Silver and Gold Particles. *Z. Physik A* **1970**, *231*, 128-143.
16. Knight, M. W.; King, N. S.; Liu, L. F.; Everitt, H. O.; Nordlander, P.; Halas, N. J., Aluminum for Plasmonics. *ACS Nano* **2014**, *8*, 834-840.
17. Yoshida, H., Near-Ultraviolet Inverse Photoemission Spectroscopy Using Ultra-Low Energy Electrons. *Chem. Phys. Lett.* **2012**, *539*, 180-185.
18. Yoshida, H., Measuring the Electron Affinity of Organic Solids: An Indispensable New Tool for Organic Electronics. *Analytical and Bioanalytical Chemistry* **2014**, *406*, 2231-2237.

19. Yoshida, H., Principle and Application of Low Energy Inverse Photoemission Spectroscopy: A New Method for Measuring Unoccupied States of Organic Semiconductors. *J. Electron Spectrosc. Relat. Phenom.* **2015**, 204, 116-124.
20. Chen, W.; Huang, H.; Chen, S.; Huang, Y. L.; Gao, X. Y.; Wee, A. T. S., Molecular Orientation-Dependent Ionization Potential of Organic Thin Films. *Chem. Mater.* **2008**, 20, 7017-7021.
21. Peisert, H.; Schwieger, T.; Auerhammer, J.; Knupfer, M.; Golden, M.; Fink, J.; Bressler, P.; Mast, M., Order on Disorder: Copper Phthalocyanine Thin Films on Technical Substrates. *J. Appl. Phys.* **2001**, 90, 466-469.
22. Cushing, S. K.; Li, J.; Bright, J.; Yost, B. T.; Zheng, P.; Bristow, A. D.; Wu, N., Controlling Plasmon-Induced Resonance Energy Transfer and Hot Electron Injection Processes in Metal@TiO₂ Core-Shell Nanoparticles. *J. Phys. Chem. C* **2015**, 119, 16239-16244.
23. Tsutsumi, J.; Yoshida, H.; Murdey, R.; Kato, S.; Sato, N., An Accurate Calculation of Electronic Contribution to Static Permittivity Tensor for Organic Molecular Crystals on the Basis of the Charge Response Kernel Theory. *J. Phys. Chem. A* **2009**, 113, 9207-9212.
24. We assume that the exponential decay function converges to the intensity of cupc without the enhancement by the nanoparticle.
25. Graber, T.; Forster, F.; Scholl, A.; Reinert, F., Experimental Determination of the Attenuation Length of Electrons in Organic Molecular Solids: The Example of PTCDA. *Surf. Sci.* **2011**, 605, 878-882.
26. Monjushiro, H.; Watanabe, I., Probing Depth of Ultraviolet Photoelectron Yield Spectroscopy in Hydrocarbon Films. *Anal. Sci.* **1995**, 11, 797-800.
27. Ozawa, Y.; Nakayama, Y.; Machida, S.; Kinjo, H.; Ishii, H., Maximum Probing Depth of Low-Energy Photoelectrons in an Amorphous Organic Semiconductor Film. *J. Electron Spectrosc. Relat. Phenom.* **2014**, 197, 17-21.
28. Gimzewski, J. K.; Sass, J. K.; Schlitter, R. R.; Schott, J., Enhanced Photon Emission in Scanning Tunnelling Microscopy. *Europhysics Letters (EPL)* **1989**, 8, 435-440.
29. Rossel, F.; Pivetta, M.; Schneider, W. D., Luminescence Experiments on Supported Molecules with the Scanning Tunneling Microscope. *Surf. Sci. Rep.* **2010**, 65, 129-144.
30. Okamoto, K.; Niki, I.; Shvartser, A.; Narukawa, Y.; Mukai, T.; Scherer, A., Surface-Plasmon-Enhanced Light Emitters Based on Ingan Quantum Wells. *Nature Mat.* **2004**, 3, 601-605.
31. Bharadwaj, P.; Deutsch, B.; Novotny, L., Optical Antennas. *Adv. Opt. Photon.* **2009**, 1, 438-483.
32. Yoshida, H., Note: Low Energy Inverse Photoemission Spectroscopy Apparatus. *Rev. Sci. Instrum.* **2014**, 85, 016101.

TOC graphic

inverse photoelectron spectroscopy



Enhancement of Signal Intensity for Inverse Photoelectron Spectroscopy by Surface Plasmon Resonance

Ryota Usui¹, Hiroyuki Yoshida^{1,2}

¹ Graduate School of Engineering, Chiba University, 1-33, Yayoi-cho, Inage-ku, Chiba, 263-8522, Japan

² Molecular Chirality Research Center, Chiba University, 1-33, Yayoi-cho, Inage-ku, Chiba, 263-8522, Japan

Supporting Information

1. Evaluation Methods of Extinction Spectra
2. Extinction Spectra of CuPc/Ag Nanoparticles
3. LEIPS Spectra of CuPc/Ag and Derivation of CuPc Contributions

1. Evaluation Method of Extinction Spectra

The photon incident to the sample is either absorbed by the sample, transmitted, or reflected. Figure S1 shows transmittance T and reflectance R of the Ag nanoparticles and the CuPc/Ag measured using the integrating sphere. We determined extinction ratio as $1 - T - R$ which is shown in Figure 2c. The obtained extinction spectrum of CuPc/Ag contains both the absorption by SPR of Ag nanoparticle and that of CuPc molecules. The further process to separate the SPR contribution is described in the next section.

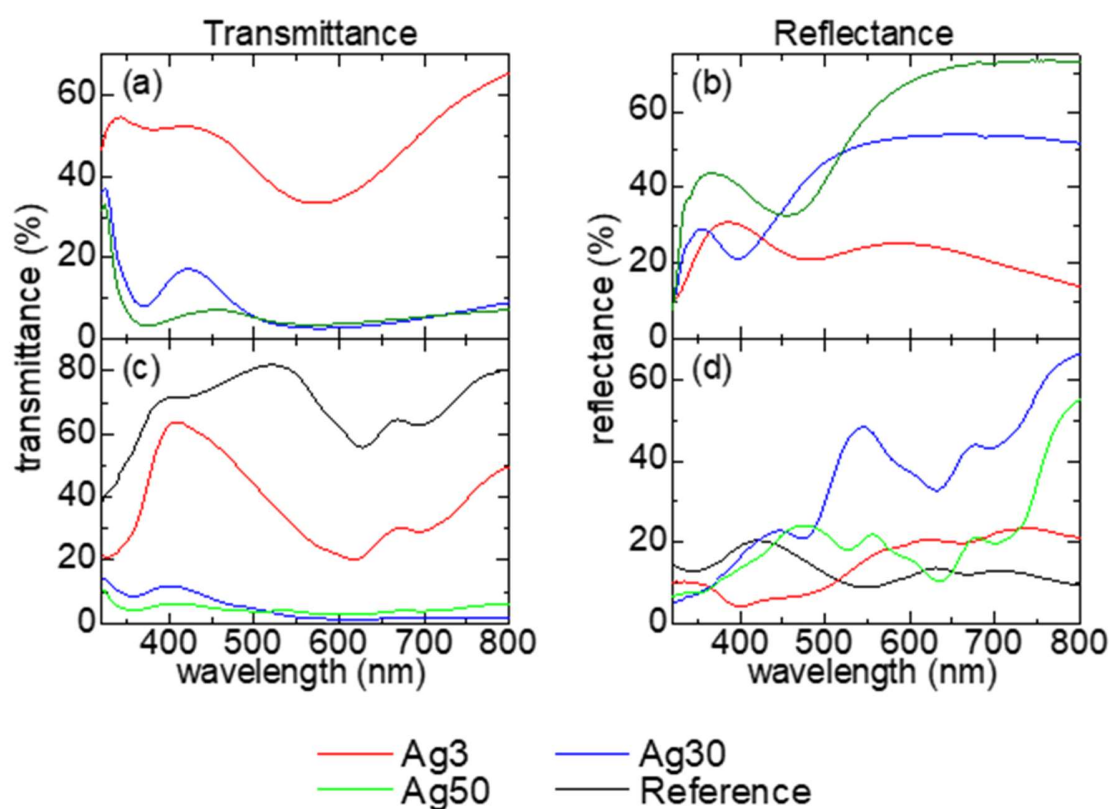


Figure S1. Results of optical measurements. (a) the transmittance and (b) the reflectance spectra of Ag nanoparticles. (c) the transmittance and (d) the reflectance spectra of CuPc/Ag.

2. Extinction Spectra of CuPc / Ag Nanoparticles

Figure S2 shows the extinction spectra obtained using the method described in the previous section. The Q-band of CuPc is clearly visible in the range between 550 and 750 nm. We remove the absorption due to the CuPc molecules from the extinction spectrum of CuPc/Ag by subtracting the log of extinction (corresponding to the absorbance) of CuPc /ITO from that of CuPc/Ag extinction spectra. The resultant extinction spectra owing to SPR of Ag nanoparticle are shown in Figure 3c.

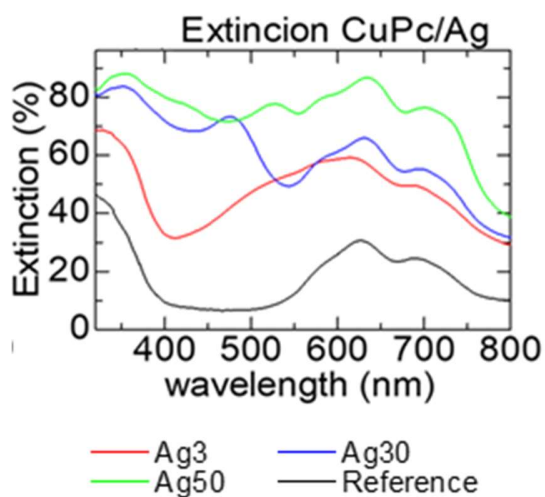


Figure S2. Extinction spectrum obtained by the procedure described in the previous section.

3. Raw LEIPS Spectra of CuPc/Ag and Derivation of CuPc Contributions

Figure S3 shows the LEIPS spectrum measured at 335 nm in wavelength as a function of average CuPc film thickness. The spectra are composed of the Ag- and CuPc-derived components. The Ag-derived spectrum shows a sharp rise at about 0.5 eV owing to the increase of the electron current and is almost constant in intensity. On the other hand, the CuPc-derived spectrum shows a peak around 1.5 eV. As the film thickness increases, the CuPc-derived intensity increases and the Ag-derived intensity decreases.

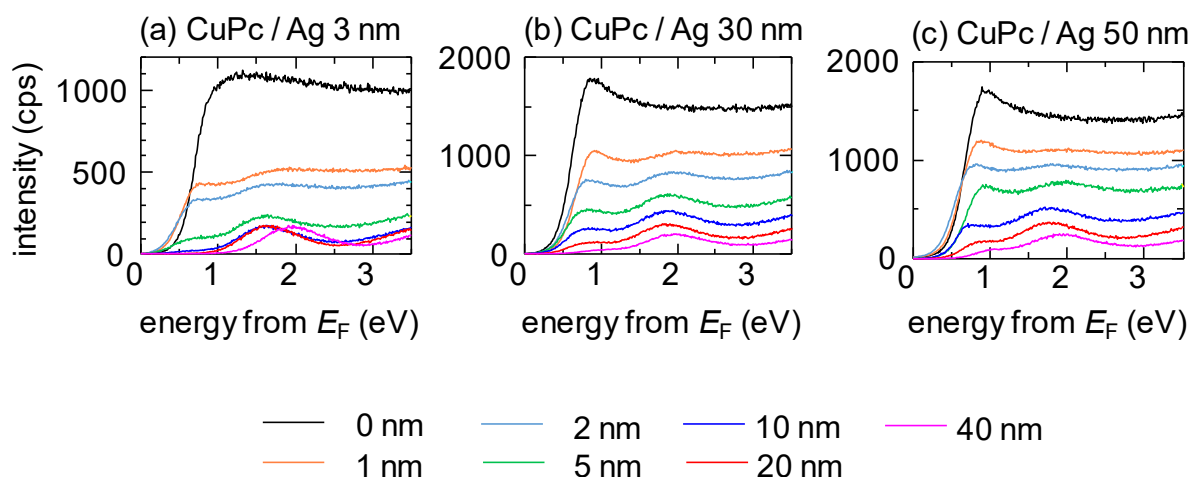


Figure S3. LEIPS spectra of CuPc/Ag films as a function of thickness. (a) CuPc/Ag3 (b) CuPc/Ag30 (c) CuPc/Ag50. The detection wavelength is 335 nm.

To discuss the enhancement by SPR of CuPc-derived LEIPS signal, we subtracted the Ag-derived LEIPS spectra from the measured LEIPS spectra of CuPc/Ag. Figure S4 shows the procedure for CuPc (5 nm) / Ag (3 nm) as an example. The spectrum of pristine Ag nanoparticles is multiplied by 0.15 so as to match the LEIPS spectrum of Ag of CuPc / Ag around the rising edge (Figure S4a). Figure S4b shows the resultant difference spectrum showing the CuPc-derived LEIPS spectra.

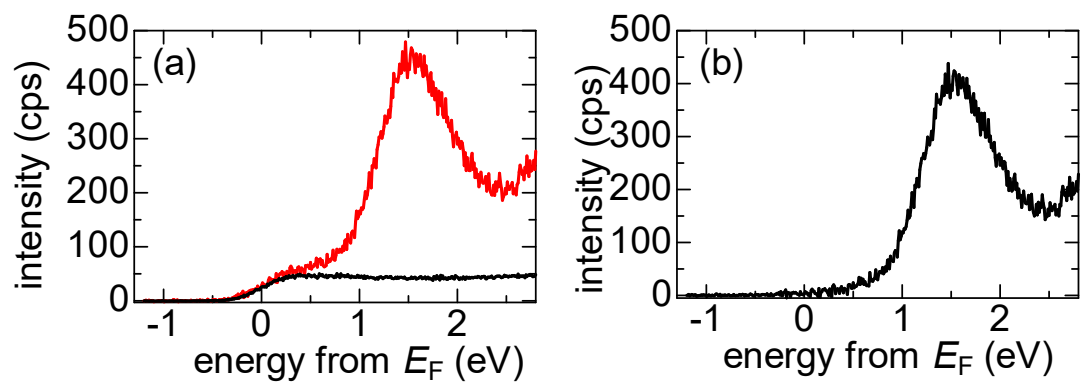


Figure S4. (a) LEIPS spectra of CuPc (5 nm)/Ag (3 nm) and Ag (3 nm) multiplied by 0.15 shown by the red and black lines, respectively. (b) Difference spectrum corresponding to CuPc-derived LEIPS spectrum.